SIMULATION OF LASER ASSISTED DOUBLE WIRE DEPOSITION WELDING WITH TWO DIFFERENT APPROACHES WITH EULERIAN (FVM) AND LAGRANGIAN (SPH) METHODS

U. REISGEN*, R. SHARMA*, O. MOKROV*,
S. EMADMOSTOUFI*, J. KRUSKA*, J. HERMSDORF**,
M. LAMMERS**, T. BOKELMANN**

**Welding and Joining Institute RWTH Aachen University, Pontstr. 49, 52062 Aachen, North Rhine Westphalia, Germany*
***Laser Zentrum Hannover (LZH) e.V., Hollerithallee 8, 30419 Hannover, Lower Saxony, Germany*

DOI 10.3217/978-3-85125-968-1-14

ABSTRACT

Laser-assisted double-wire deposition welding is a welding process developed at LZH to increase the deposition rate with the minimum degree of dilution of the surfacing layer. The use of the laser beam serves to locally heat up the molten pool and substrate surface and, thanks to a smaller wetting angle, leads to improved bond to the substrate, which causes a wider and deeper weld pool. The aim of this paper is to investigate the basics of this process using numerical methods. The free surface of the deposition layer, the mass flow of the melting wires in the weld pool, as well as interphase mass exchange (e. g. evaporation), laser absorption and interphase heat balance were calculated. Two different simulation methods Eulerian finite volume method (FVM) and Lagrangian smooth particle hydrodynamics (SPH) were used to build the model. This paper deals with the model construction as well as the precision and computational effort of these methods. The results of both methods agree with each other. Conclusions were drawn about the advantages and limitations of both methods

Keywords: Laser-assisted double-wire deposition welding, simulation method, FVM, SPH, Eulerian, Lagrangian

INTRODUCTION

Laser assisted double wire welding with non-transferred arc (LDNA) is a process developed by Laser Zentrum Hannover (LZH) for metal deposition and surfacing. In this process, the arc is ignited between two continuously fed wire electrodes. The wire electrodes melt and the droplets fall onto the substrate surface. This process offers not only a low degree of dilution, but also a high deposition rate.

The droplets, depending on the size, temperature and velocity and their falling trajectory, can affect the weld pool hydrodynamics. Heat and volume of dripped metal

adds heat into the weld pool. Size, velocity and direction of the molten droplets lead to additional momentum into the welding pool.

To improve the connection of the cladding layer, a laser beam oscillates transversely to the welding direction. This oscillation leads to an improved wetting angle on the sides with local heating of the weld pool, especially at the edges, and avoids the undercut formation (Fig. 1).

Because of the local heating of the laser beam, the melt evaporates partially on the surface of the melt pool. In addition, this heating affects the local temperature of the melt pool surface and thus the surface tension, which in turn causes additional convection due to the Marangoni effect. The absorption of the laser beam depends on the angle of the incident beam and the temperature of the free weld pool surface. The physical phenomena are shown in the Fig. 2.

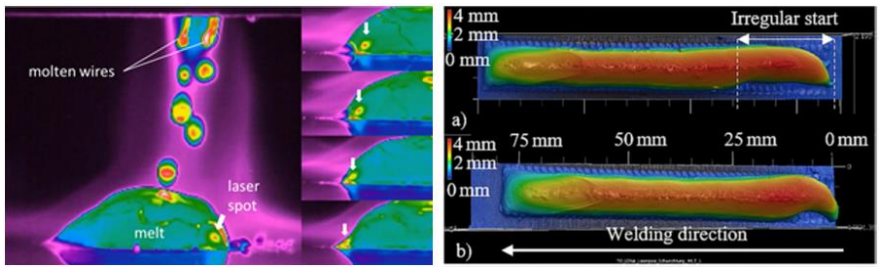

Fig. 1 Left, falling droplets and local heating by laser during the LDNA process, captured transvers to weld direction by thermal camera, colours represent different temperatures. Right, the solidified weld seam topology with laser scanning microscopy (LSM), the colours illustrate the height of deposited layer

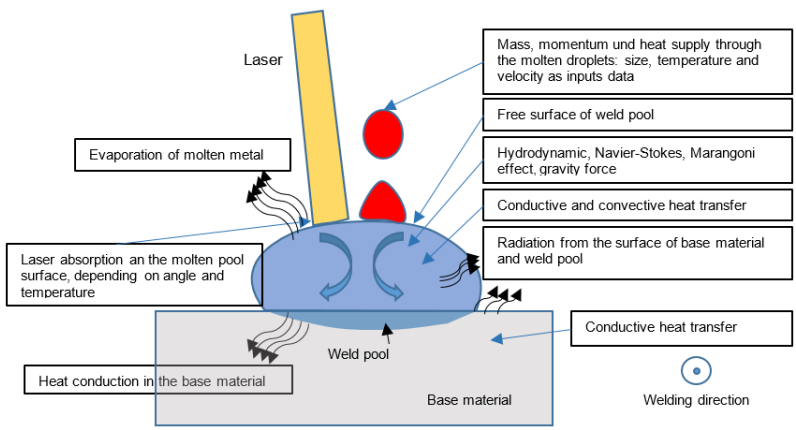

Fig. 2 Schematic cross section, explanation of all to be simulated phenomena of the process

For the simulative investigation of the LDNA process two different models based on differing approaches are developed. The first one, finite volume method (FVM), as an Eulerian method, implemented in ANSYS CFX® is compared with the Lagrangian method Smoothed Particle Hydrodynamics (SPH).

The SPH is a mesh-free Lagrangian method, which in recent years has received growing attention for the investigation of fluid dynamics problems. SPH is particularly well suited for the modelling of free surfaces, since those are handled implicitly by the discretization technique, which makes it an appealing method for the investigation of welding simulations. In this work the open source SPH frameworks SPlisHSPlasH [1] is used. The framework has an extended library to allow heat transfer, physical surface phenomena, viscous fluid behaviour and simplified solidification calculations. It has previously been used for the simulation of manufacturing processes, especially the problem of fluid mass and heat transfer in [2, 3]. It allows the development of a simulation model of the LDNA process.

Furthermore, the aim is that the algorithms developed for this work will be integrated into the main SPlisHSPlasH framework.

STATE OF ART

In order to experimentally investigate the process, number of experimental tests, which have been described earlier in [4–8], were carried out. The physical phenomena that occur in this process have not been determined in a simulation so far. This investigation is the computer-aided description of this process. However, there are various simulative tests for other similar welding processes. Often equivalent heat sources are used for thermal modelling of deposition welding, for example, Amal et al. [9] used equivalent heat source to calculate the residual stresses in "Wire arc additive manufacturing" using commercial software Simufact. Zheng et al. [10] built up numerical model for regulation of heat input and Nikam et al. [11] tried the thermal analysis of multilayer metallic deposition during plasma arc based additive manufacturing. Chai et al. [12] implemented the laser powder interaction in a thermal analysis with cellular automaton in laser cladding process. Although their results show good geometric agreement with the real process, they cannot precisely determine the temperatures in cross-sections. Han et al. [13] investigated on hybrid laser and submerged arc cladding, and simulated the resulting residual stresses. Zhang et al. [14] considered the hydrodynamic and microstructure evolution in laser cladding process using a coupled model of FEM and cellular automaton.

Song et al. [15] investigated on the internal molten flow convection on evolution of the solidification. They also believe that the Marangoni effect has a magnificent influence on the cladding layer.

Eulerian methods are very common for the simulation of arc welding processes and have been used since the advent of computational welding simulation. A common difficulty in these methods is the calculation of free surface flows. There are several numerical approaches which are commonly used for the description of these free surface flows. They can be divided into two main groups [16]. The first group includes the so-called Front Capturing Methods (FCM) in which a fixed Eulerian computational mesh is employed and a free surface is”expanded” along the volume of a certain layer. The thickness of this layer corresponds to several lengths of a computational cell. The most popular FCM are Volume of Fluid (VOF) [17, 18] and Level Set (LS) [19] methods. There also exists a number of other approaches where the free surface is considered as a sharp interface between two media, e.g., [20–22]. There the Arbitrary–Lagrangian–

Eulerian method (ALE) is used, which allows the deformation of the mesh, but it does not allow to solve problems with significant topological changes, like flow-splitting. However, most common arc welding processes involve a melting, detachment and an impingement of a filler material into a weld pool. Both the approaches, the VOF/LS and the ALE are only limited satisfactory to accurately capture the process. Due to its strengths in modelling free surfaces as well as considering discontinuities and large topological changes and deformations, the SPH method became an interesting approach for modelling arc welding processes. However, a very little is known yet about the quantitative performance for the calculation of conductive/convective heat transfer compared to the established Eulerian methods, in the context of arc welding processes.

SMOOTHED PARTICLE HYDRODYNAMICS FOR WELDING PROCESS SIMULATION

The smoothed particle hydrodynamics (SPH) method was originally proposed by Lucy [23] and Gingold and Monaghan [24] in the field of Astrophysics. Since then it has been adopted for many different applications, including the simulation of weld pool dynamics. The mesh-free nature of SPH enables the simulation of large deformations, free surface motion and coupling of many physical processes, which makes it an attractive method for many real-world problems.

Das and Cleary [25] use SPH in three-dimensional arc welding simulations in order to study temperature distributions, flow patterns and plastic strain in the filler material and residual thermal stresses in the work piece. Ito et al. [26] perform full simulations of tungsten inert gas (TIG) welding using the SPH method and show results for different material properties due to different sulphur contents and evaluate the flow patterns and the shape of the weld pool.

Trautmann et al. [27] similarly perform weld pool simulations using SPH for a TIG welding process. They consider buoyancy, viscosity and surface tension as flow driving forces and the arc pressure, shear and all relevant thermal effects were parameterized using experimental studies. The penetration profiles of three different welding currents were compared to experimental results and decent agreement was shown. A hybrid approach is investigated by Komen et al. [28], who use an Eulerian grid and Lagrangian particles in conjunction, in order to simulate gas metal arc welding (GMAW). Molten metal is simulated by means of SPH, while the arc plasma and gas are simulated on a grid. The methods are then weakly coupled and executed iteratively.

Komen et al. [29] also simulate the GMAW process under consideration of droplet formation and compare the weld pool shapes against experimental results. In order to visualize results more easily, they use an ensemble averaging in order to transfer particle data onto a regular grid. These types of simulations are difficult to validate, as they describe very complex systems with many interacting components, and this is evident with Trautmann et al. [27] being one of the few works which attempts to validate their results using experimental data. In this paper, we choose to compare our proposed SPH method against Eulerian simulations, as a proof of concept which shows that SPH is able to obtain very good agreement in the resulting weld pool shapes, as well as temperature and velocity distributions. Similar comparative studies were conducted by Jeske et al. [2, 3]. In [2] excellent results of the SPH method when compared against the Eulerian VOF

method for the simulation of droplet impacts in thermal spraying were obtained. In [3] the Eulerian and SPH methods were compared regarding the simulation of flows arising under the action of the Lorentz force with variable distributions of electric current density during tungsten electrode welding. A remarkable agreement between the melt pool shapes, which are highly dependent upon these forces, is shown. This allows to justify the usage of SPH to obtain physically meaningful results, especially for cases that pose more difficulty for Eulerian methods, for instance when considering free surfaces. The studies carried out confirm the qualitative accuracy of the proposed method as well as the SPH method in general for such applications.

MODEL

GENERAL MODEL ASSUMPTIONS

Both variants of the model are based on the following general assumptions:

- Molten metal is a Newtonian, incompressible, laminar fluid
- The Arc is not transferred to the molten metal in the LDNA process, therefore, the electromagnetic forces and arc are not modelled. The focus lies on the droplet behaviour during falling, without consideration of formation of the droplets in the arc.
- Droplet behaviour (spatial velocity, temperature, size) has been measured using a thermal camera.
- Gravity and its influences on the falling droplets and on natural convection in gas phase as well as in molten metal is considered.
- The solidification is modelled using the enthalpy porosity method.
- For the evaporation, mass loss is excluded. (Euler's method can account for mass loss, but the SPH method needs further development for this goal)

Some differences at a glance:

- In Euler’s method, the molten metal is in interaction with surrounding gas phase. In SPH, the gas phase was excluded.
- The scattering of the laser beam in Euler's method is isotropic, but was not taken into account in SPH.
- The Marangoni effect as a result of the temperature dependent surface tension was taken into account in Euler's method but not in the SPH because of the constant surface tension with corresponding SPH development status.
- The hydrodynamics in the melt pool was taken into account in both models, but in Euler's method it is a result of the droplet momentum and the density variation with temperature, but in SPH the density is considered constant, therefore the hydrodynamics are only affected via droplet momentum.

The enthalpy-porosity approach [30, 31] is used in both the SPH and FVM simulations. This method aims to precisely model the flow during the solidification by introducing an

additional deceleration in the Navier-Stokes equation for material between the solidus and liquidus temperature. Because of that it is sometimes referred to as a momentum loss or momentum sink.

The symbols used in the mathematical model are listed in the Table 1.

Table 1 Symbols used in the mathematical model chapter

Symbol	Definition	Symbol	Definition
$\vec{v}$	Velocity vector in momentum equation	I_0	Energy of incident radiation on the surface
p	Pressure	$I(z)$	Energy of transmitted radiation in depth z
η	Dynamic viscosity	l	Path length of transmission
λ	Lame constant	$\dot{M}_w$	Wire mass rate
$\vec{f}$	Gravity	$\dot{M}_d$	Droplet mass rate
S_s	mass source of shielding gas	v_w	Wire feeding speed
S_m	mass source of molten metal	A_w	Wire cross section area
T	Temperature	R_w	Radius of wire
k	Heat conductivity	R_d	Radius of droplet
C_p	Specific heat capacity	V_d	Volume of droplet
ρ	Density	v_{d1}	Frequency of inflow of drops 1
v	Velocity	v_{d2}	Frequency of inflow of drops 2
q_{vol}	Volume heat source in energy equation	s_{d1}	Switch function I/O of droplet 1
q_{rad}	Volume heat source via Radiation	s_{d2}	Switch function I/O of droplet 2
T_0	Ambient temperature	Θ	Step function
q_b	Volume heat source for laser beam	ρ_m	Density of molten metal
P	Laser beam power	f_{d1}	Normalisation factor of mass for droplet 1
μ	Attenuation coefficient	f_{d2}	Normalisation factor of mass for droplet 2
μ_a	Absorption coefficient	$\dot{m}_{d1}$	Mass flux of droplet 1
μ_s	Scattering coefficient	$(\dot{m}_{d1})'$	Mass flux of droplet 1 with irregularity
$a(T)$	Temperature dependent absorption fraction	$\dot{m}_{d2}$	Mass flux of droplet 2
Tr	Transmittance	$(\dot{m}_{d2})'$	Mass flux of droplet 2 with irregularity
d_d	Droplet distance	$c_{p,m}$	Specific Heat capacity of molten metal
$(d_d)'$	Droplet distance with irregularity	T_b	Boiling temperature
v_x	Drop velocity in longitudinal direction (x)	L_b	Latent Heat of evaporation
v_y	Drop velocity in transverse direction (y)	$\dot{m}_e$	Mass flux of evaporated metal
v_z	Droplet speed in height direction (z)	δt	Time increment
v_{xz}	Diagonal drop speed in xz plane	$\mathcal{N}$	SPH neighbourhood relation
v_{xyz}	Diagonal droplet speed	$\mathcal{N}_x$	Set of neighbours at location x

α	Droplet angel over longitudinal direction	V_i	Volume of particle i
$\dot{q_e}$	Heat flux of evaporation	A_i	Arbitrary quantity A of particle i
β	Droplet angel over transversal direction	$W(x;h)$	SPH smoothing kernel
v_p	Droplet parallelity frequency	h	Smoothing radius
M_x	longitudinal momentum loss	χ	Coverage angle
M_y	Transversal momentum loss	φ	Laser angle to altitudinal direction
M_z	altitudinal momentum loss	$C(x)$	SPH color field
C	Morphological constant	κ	curvature
s_m	Activation switch for Momentum Loss	γ	Surface tension coefficient
u_x	fluid velocity in longitudinal direction (x)	T_i	Temperature of particle i
u_y	fluid velocity in transverse direction (y)	$\dot{q}$	Heat flux in Lagrangian approach
u_z	fluid velocity in height direction (z)	r_l	Heat source radius
v_w	Welding speed	r	Distance from centre of Gaussian
ϕ_m	Volume of fluid of molten metal	ϵ	Emissivity
T_m	Temperature of molten metal	σ	Stefan Boltzmann constant
T_s	Solidus temperature	h	Heat transfer coefficient
T_l	Liquidus temperature	r_p	Particle radius
w_e	Mass Fraction of evaporated metal	n	Surface normal

EULERIAN APPROACH

GEOMETRY AND BOUNDARY CONDITIONS IN EULERIAN APPROACH

The model contains two domains, the substrate (the lower one) which consists of the base material and the cladding layer (the upper one), see Fig. 3. The cladding layer consists of the incoming molten metal, the shielding gas and the metal vapour in a varying combination. The base material, as fluid (see 4.2), flows through the substrate domain with the welding velocity in moving coordinate system. The melt adheres to the contact surface between the cladding layer and the substrate. The top and lateral sides of the upper domain are described as open with a relative pressure of 0 [Pa] and a black body temperature of 300 [K]. The upper surface has the unity volume fraction of gas mixture with the shielding gas mass fraction to be 1 and the beam source of the laser as the Monte Carlo method of boundary condition. This is a ANSYS CFX implemented method of "ray tracing" in which material is irradiated with a certain number (here 10000) energetic rays and depending on the angle of incidence and the radiation properties of material (absorption and scattering) these are absorbed or scattered.

Except for the contact surface with the coating layer, the other surfaces in the substrate are defined as frictionless (slip wall), which loss the heat with convection (heat transfer coefficient) and radiation (Stefan Boltzmann's law).

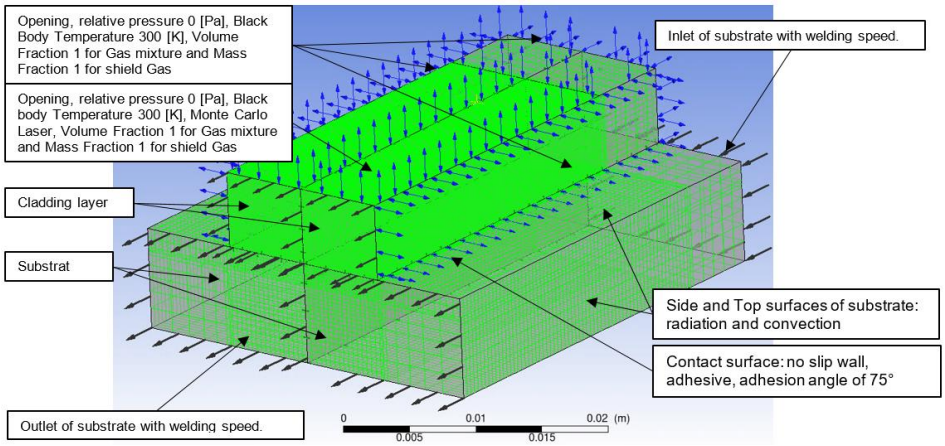

Fig. 3 Domain geometry, meshing and boundary conditions

Droplets drop diagonally from right side to molten pool (Fig. 6 & Fig. 7), so the hydrodynamics and solidification front would not be symmetrical. Therefore, we could not use symmetrical geometry and meshing, and the problem should be solved in the whole domain.

MATHEMATICAL MODEL

In this paper, the authors used FVM in multiphysics multiphase model with inhomogeneous heat and mass transfer with consideration of hydrodynamics and convection in the molten pool, Marangoni effect, radiation from the molten pool and solidified cladding layer to ambient and secondary heat gained via scattered laser beam.

Although the Euler approach is suitable for implementing some phenomena like evaporation of molten metal due to oscillating of laser beam, heat gain and loss via shielding gas flow in and out of arc area and heat radiation of the arc on the molten pool, these were not taken into account in the model, because the main aim of this article is to compare the FVM Eulerian and the SPH Lagrangian method.

In order to be able to simulate both physical states of material (solid and liquid) in a moving coordinate system, both physical states of metal are described as fluid. This type of implementation is typical for ANSYS CFX. In addition, during and after solidification, the increasing viscosity and enthalpy porosity result in damping the flows, so that the solidified fluid is numerically still a fluid, but behaves like a solid.

The cladding domain consists of molten metal and gas (mixture of shielding gas and metal vapour). These phases should be separated from each other via the free surface task. The Volume of Fluid (VOF) method is used to calculate the free surface of the molten metal. The volume fraction of the melt in each cell is described as follows:

- $VOF = 1$, there is only molten metal in the element
- $VOF = 0$, there is only gas (mixture of shielding gas and metal vapour) in the element

- $0 < VOF < 1$, melt fills only a part of an element, thus it forms the free surface of molten pool.

There should be some cells between VOF 0 and 1 (Fig. 4). This requires very fine meshing wherever the melt pool surface is formed during the process. This results in a very high computational effort in this method. The surface tension plays an important role and the Marangoni effect is also taken into account due to the temperature-dependent description of the surface tension.

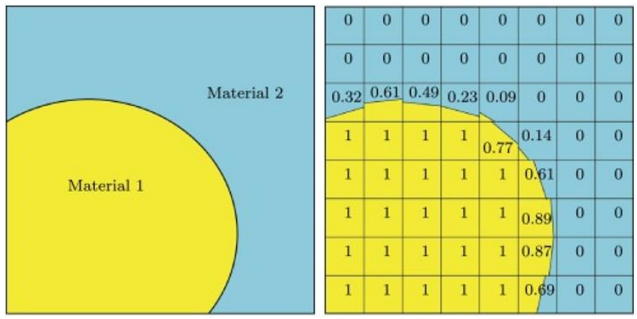

Fig. 4 The schematic volume of the fraction to model the free surface between two media [32]

The mass flux of the inflowing droplets into the domain results from the mass conservation of the melted wires. The frequency of the mass supply of the droplets into the domain is described on the basis of the measured droplet size and sphere shape via thermal camera. Therefore, droplets are modelled also spherical, and defined in the model with Gaussian mass distribution for numerical reasons.

Navier-Stokes equation for incompressible molten metal

$$\rho \frac{D\vec{v}}{Dt} = \rho \left(\frac{\partial \vec{v}}{\partial t} + (\vec{v}.\nabla)\vec{v} \right) = -\nabla p + \mu \Delta \vec{v} + (\lambda + \mu)\nabla(\nabla.\vec{v}) + \vec{f} \tag{1}$$

Mass balance equation (continuity):

$$\frac{D\rho}{Dt} = \frac{\partial \rho}{\partial t} + \nabla \rho = S_s + S_m \tag{2}$$

Energy equation:

$$C_p \rho \frac{\partial T}{\partial t} = \nabla(\lambda \nabla T) - \nabla\left(\rho C_p v T\right) + q_{vol} \tag{3}$$

$$q_{vol} = q_h + q_{rad} + q_b \tag{4}$$

$$q_{rad} = \varepsilon \sigma (T^4 - T_0^4)\delta \tag{5}$$

$$q_h = h(T - T_0)\delta \tag{6}$$

$$\delta = \sqrt{(\nabla \phi_m)^2} \tag{7}$$

$$q_b = \frac{\mu P}{\pi R_b^2} \tag{8}$$

As the materials (substrate and cladding layer) are not transparent, the laser beam does not get transmitted through the medium. Therefore, attenuation coefficient results from the sum of absorption and scattering.

$$\mu = \mu_a + \mu_s \tag{9}$$

$$\mu = -\frac{1}{l} ln(Tr) \tag{10}$$

$$Tr = \frac{I(z)}{I_0} = assumed\ as\ e^{-4}\ in\ path\ length\ 1\ [mm] \tag{11}$$

$$\mu_a = a(T)\mu \tag{12}$$

$$\mu_s = (1 - a(T))\mu \tag{13}$$

As already mentioned, the Monte Carlo method can take into account the angle of incidence and the absorption and scattering properties of the medium. One can add a temperature dependency to the Monte Carlo method by using the temperature-dependent absorption fraction.

Mass source:

$$\dot{M}_w = \dot{M}_d \tag{14}$$

$$v_w A_w = \dot{n}_{d1} V_d \tag{15}$$

$$\begin{cases} \upsilon_{d1} = \frac{v_{w1} A_{w1}}{V_d} \\ \upsilon_{d2} = \frac{v_{w2} A_{w2}}{V_d} \end{cases} \qquad A_w = \pi R_w^2 \ , \quad V_d = \frac{4}{3}\pi R_d^3 \tag{16}$$

In order to develop drop-like mass flow, the mass source is time-modulated. The general on/off function can be written as follows:

$$s_d = \Theta\left(0.5\, Sin\left(2\pi \upsilon_{d1}(t + \frac{\xi}{2\pi \upsilon_{d1}})\right) + 0.5 - |sin(\xi)|\right) \tag{17}$$

Here ξ=64° was assumed

$$s_{d1} = \Theta\left(0.5\, Sin\left(2\pi \upsilon_{d1}(t + \frac{\arcsin(0.9)}{2\pi \upsilon_{d1}}\right) - 0.4\right) \tag{18}$$

$$s_{d2} = \Theta\left(0.5\, Sin\left(2\pi \upsilon_{d2}(t + \frac{\arcsin(0.9)}{2\pi \upsilon_{d2}}\right) - 0.4\right) \tag{19}$$

The on/off switch function within the laser period (T=0.05 [s]) can be seen in the Fig. 5.

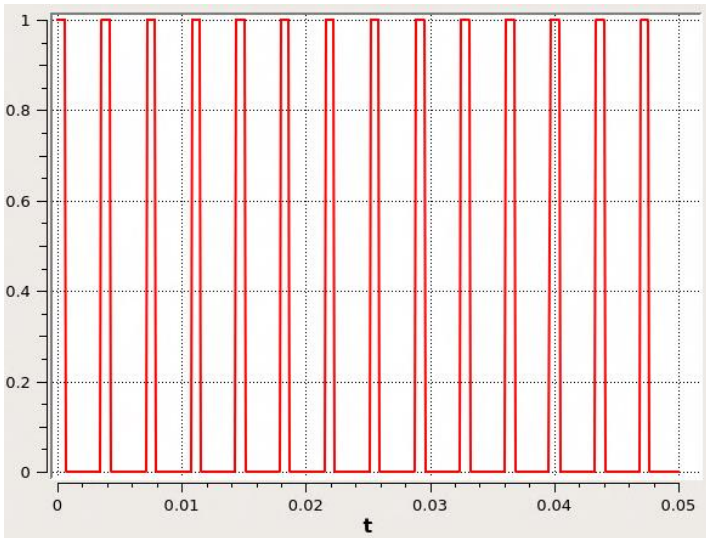

Fig. 5 Switch function of first wire droplets in mass flux function

The above function turns on the mass flow source of the drops only a fraction of the time. To ensure the mass conservation of the melted wires, the function shall be normalized and the integration in one second gives 1: Therefore, the mass rate function is settled with the following factor:

$$f_{d1} = \left(\int_0^1 s_{d1} dt\right)^{-1} = 5.605 \tag{20}$$

$$f_{d2} = \left(\int_0^1 s_{d2} dt\right)^{-1} = 5.218 \tag{21}$$

The mass flux is found as follows:

$\dot{m}_d$ = Normalising factor × time switch × droplet mass × number of droplets ×mass distribution

$$\dot{m}_{d1} = 8\sqrt{3}\, f_{d1}\, s_{d1}\, \rho_m\, \upsilon_{d1}\, exp\left(\frac{-3}{R_d^2}((x-x_{01})^2 + (y-y_0)^2 + (z-z_0)^2)\right) \tag{22}$$

$$\dot{m}_{d2} = 8\sqrt{3}\, f_{d2}\, s_{d2}\, \rho_m\, \upsilon_{d2}\, exp\left(\frac{-3}{R_d^2}((x-x_{02})^2 + (y-y_0)^2 + (z-z_0)^2)\right) \tag{23}$$

$$x_{02} = x_{01} + d_d \tag{24}$$

At the beginning of the process, when the arc is ignited, the process can be unstable and the droplets are twice as large in diameter. Therefore the droplets have eight times the volume. In order to map this time in the simulation, we can change the mass flux and droplet distances for a so-called irregularity time, t_i as follows:

$$(\dot{m}_{d1})' = \dot{m}_{d1}(1 + 7\Theta(t_i - t)) \tag{25}$$

$$(\dot{m}_{d2})' = \dot{m}_{d2}(1 + 7\Theta(t_i - t)) \tag{26}$$

$$(d_d)' = d_d + 0.5\Theta(t_i - t) \tag{27}$$

The measurement of the drop velocity (v_{xz}) is carried out by recording a high-speed camera (Fig. 6) and analyzing the frame rate and the distance covered by the drops. The angles of the droplet trajectory across the transverse (β) and longitudinal (α) directions are measured using two mounted cameras (Fig. 7). The projection of the droplet velocity in the longitudinal and vertical and transvers directions is calculated using the analysis of the recordings of the two mentioned mounted camera as follows:

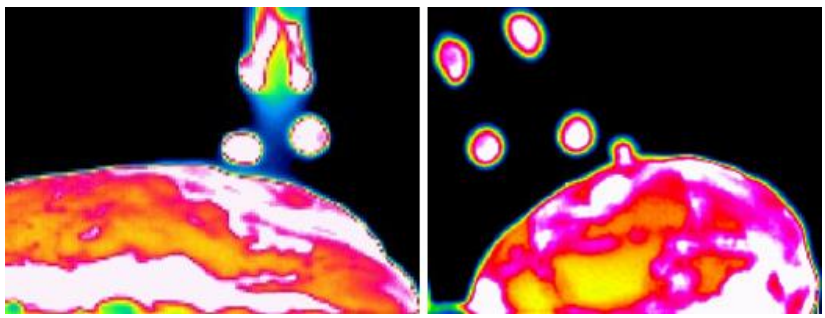

Fig. 6 Droplet size and trajectories, left: over longitudinal direction (camera transverse) and right: over transversal direction, (camera in welding direction)

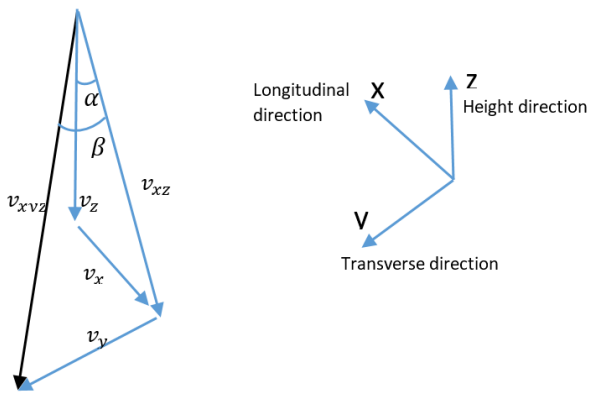

Fig. 7 Velocity vectors in longitudinal, transversal and altitudinal directions

$$v_{xz} = v_{xyz}\cos(\beta) \tag{28}$$

$$v_y = v_{xyz}\,sin(\beta) = v_{xz}\,tan(\beta) \tag{29}$$

$$v_z = -v_{xz}\,cos(\alpha) \tag{30}$$

Since the drops have opposite directions about the longitudinal axis, then:

$$v_{x1} = -v_{xz}\, sin(\alpha) \tag{31}$$

$$v_{x2} = v_{xz}\, sin(\alpha) \tag{32}$$

The angle of the drops of the respective wires to the height axis (longitudinal velocity) varies constantly, so that the drops diverge (opposite direction) or converge and have parallel trajectories in the course of the process.

Therefore, the angle α is sinusoidal and time-dependent as follows, in which v_p describes the frequency of how often the drops diverge or converge.

$$\alpha = 5\, sin\left(2\pi v_p\left(t - \frac{1}{4v_p}\right)\right) + 5 \tag{33}$$

After solidification, the velocity vectors should only show the welding speed of the sheet metal. In order to dampen the velocity vectors in the solidified layer, the enthalpy porosity method is used as follows:

$$M_x = -C\, s_m(u_x - v_w) \tag{34}$$

$$M_y = -C\, s_m(u_y) \tag{35}$$

$$M_z = -C\, s_m(u_z) \tag{36}$$

In which s_s is the switch to activate momentum loss function for temperatures below the melting point and volume fractions above 0.5:

$$s_m = \Theta(\phi_m - 0.5)\Theta(T_s - T_m) \tag{37}$$

For the representation of evaporation, the mass and heat balance of evaporation should be implemented as mass and heat source. Mass fraction of the vaporized metal from temperatures above the boiling point results from the ratio of the absorbed enthalpy to the latent heat:

$$w_e = c_{p,m}(T_m - T_b)\Theta(T_m - T_b)/L_b \tag{38}$$

The evaporation mass flux results from the mass fraction of the vaporized metal and the available molten metal mass per volume in the cell (product of density and volume of fraction) divided by time:

$$\dot{m}_e = w_b \phi_m \rho_m / \delta t \tag{39}$$

The evaporation is calculated from the evaporation mass flux and the latent heat of evaporation:

$$\dot{q}_e = \dot{m}_e L_b \tag{40}$$

SMOOTHED PARTICLE HYDRODYNAMICS

The smoothed particle hydrodynamics method was adapted to the problem of fluid dynamics by Müller et al. [33]. It is a mesh-free method, i.e. it does not require connectivity information between discretization points. The absence of explicit connectivity information through a mesh lifts one of the major limitations of mesh-based methods, namely the limitation of possible movement of the discretization points. In contrast to mesh-based methods, mesh-free methods allow for free movement of the discretization points. This, in turn enables movement of the discretization points according to the velocity field, i.e. enabling a Lagrangian treatment of the underlying fluid.

SPH is one of the most widely adopted Lagrangian methods, where physical quantities are discretized onto a set of freely mobile discretization points. Each of these points carries the physical quantities associated with it as it moves according to the velocity field. The points are often thought of and visualized as particles by associating a certain spatial extent with each discretization point, hence the name smoothed particle hydrodynamics. In lieu of a mesh for connectivity information and since interactions between "close" points are necessary for a physically accurate simulation, SPH makes use of a neighbourhood relation $\mathcal{N}$. Complete pairwise interactions between all particles in a simulation is computationally infeasible, therefore SPH typically utilizes an efficient search structure to determine neighbourhoods such as the one presented in [34], as well as limiting the sizes of these neighbourhoods.

In SPH an arbitrary quantity $A(\vec{x})$, that was discretized onto particles can thus be computed by interpolating the local neighbourhood $\mathcal{N}_{\vec{x}}$ of the sample point $\vec{x}$:

$$A(\vec{x}) = \sum_{j \in \mathcal{N}_{\vec{x}}} V_j A_j \, W(\vec{x} - \vec{x_j}; h) \tag{41}$$

This kernel function is used as a weighing scheme for particles depending on their spatial relation to the sample point. Generally particles that are further away from the sampling point, have a lower contribution to the quantity $A(\vec{x})$, than nearer particles. This weighing results in a smoothed field $A(\vec{x})$, hence the name smoothed particle hydrodynamics. A well-known function that could be used as a kernel would be the Gaussian function. However, it has one disadvantage, namely that it has infinite support, which means all particles in the simulation would add small contributions to any interpolation. As noted before the number of contributing particles should always be large enough for good interpolations, but as small as possible such that the interpolation is efficiently computable. Therefore, the most frequently used kernel functions have a finite support and are scaled according to the smoothing length parameter h, such that only a small number of particles, namely those for which $||\vec{x} - \vec{x_j}|| < h$, need to be considered for the interpolation. In this paper the cubic spline kernel [35] is used.

It is important to note that the SPlisHSPlasH library itself is an ongoing research project in active development. As such there are many physical phenomena that are not yet taken into account, either due to lack of existing implementations within SPlisHSPlasH, or a lack of well-founded methods for their modelling in SPH in general. As such simpler compensation models were developed and applied for the LDNA SPH simulation. Despite these, often rather crude compensation models, we were able to show

remarkable results for the SPH simulation of the LDNA process including very good agreement with the simulation in ANSYS CFX.

Since SPH has been adapted to the problem of fluid dynamics, a large number of methods have been proposed for various phenomena, typically associated with fluid dynamic simulations, e.g. pressure, viscosity and surface tension solvers. Beyond that however, there are several important physical phenomena that arise in welding simulations, which are not part of the typical SPH repertoire. This includes thermal effects, such as heat in- and outputs, thermal conduction and a solidification/melting model, electromagnetic effects, such as Lorentz forces for droplet detachment and melt pool flows.

Nonetheless, they are crucial and some treatment of these phenomena is necessary to obtain accurate welding simulations.

BOUNDARY CONDITIONS IN SPH AND MOVING DOMAIN OF MASS AND HEAT FLUX

In contrast to Eulerian approaches, where the need to discretize and solve the entire domain generally places quite significant restrictions on the potential, the domain in SPH is theoretically and practically unbounded (Fig. 8 & Fig. 9). This is due to the fact, that equations are only solved at particle locations, i.e. only where material exists. As a consequence, large but sparse and potentially even unbounded domains are very feasible. On the other hand, many boundary conditions that are easily formulated in an Eulerian frame are more complicated to realize in a Lagrangian one, most importantly here are mass in- and outlets. As such mimicking the welding movement by a mass inlet and outlet parametrized by the welding speed, as it was done in the FVM simulation, is not a very natural formulation for the SPH simulation.

Rather in SPH it is much more appropriate and easier to keep the substrate fixed, and moving the wire mass source according to the welding speed instead. The relative movement between substrate and wire mass source remains the same, however the absolute frame of reference differs between the simulations.

Furthermore, this means that many other effects are defined relatively to the mass source, such as droplet acceleration and the position of the laser. In the moment this movement is a uniform horizontal movement for both wires along the weld direction as specified by the welding speed.

As already stated the SPH interactions are only calculated between particles, therefore SPH boundary conditions are free-slip by default, unless additional effects, that change boundary behaviour, are specified. As this was the condition for FVM there was no reason to change it in the SPH simulation.

Since SPlisHSPlasH currently forbids movement of any particles below the melting temperature, gravity does not affect the solid material.

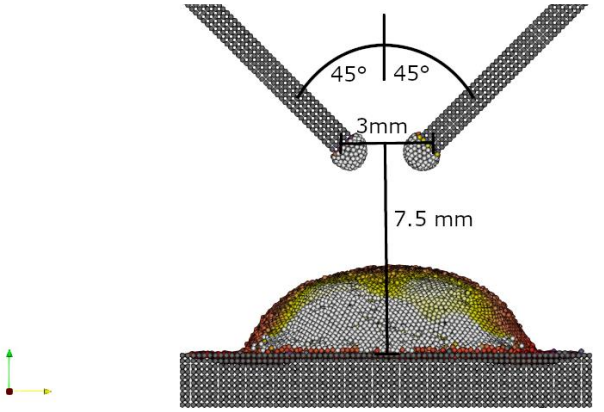

Fig. 8 Front view of simulation geometry with schematic arrangement annotations

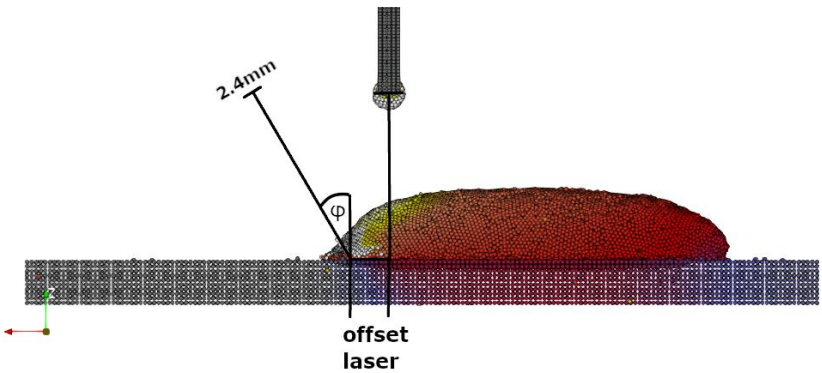

Fig. 9 Side view of simulation geometry. φ and laser offset are variable parameters

Molten material with a temperature of T (In this case 2100 K, according to experimental measurements) drops on the surface, which constitutes mass and energy addition into the cladding layer. Secondly, the laser/heat-source constitutes another energy input into the substrate and cladding layer. Lastly convection between material and air, as well as thermal radiation at the material surface constitute an energy loss of the system.

DENSITY

Arguably the biggest limitation of the framework for the purpose of welding simulations is the lack of variable density. Currently, a material can have a single density, independent of its temperature. However, since density is closely related to the pressure solver of SPH, the implementation of the temperature dependant density is under development in the current solver. In the current state of the simulation framework, either mass or volume will deviate from observed values. Whether mass or volume are

determined accurately and whether over- or underestimates of the other are made is up to the user, depending on the values and compensation models used. Treating mass correctly was deemed to be of higher priority, such that accuracy regarding energy models is retained. As such the entire material is assumed to have a density of molten steel (6793.7 kg/m^3) and the push speed of the welding wire is adjusted upwards by a factor around 7948.9 / 6793.7 ≈ 1.17, such that mass gain of the simulation is correct. This results in correct mass and volume for molten regions, but an overestimation of volume by roughly 15 % for the solidified welding seam. Even if the consideration of the density change is algorithmically possible, this assumption is often used for the simulation of the flows in the melt pool, since the correct consideration of the density change causes massive additional calculation work.

WIRE MASS SOURCES AND MOVEMENT

As stated previously that the wire mass sources are the moving reference points. Since the domain in SPH is not restricted, it is also entirely feasible to initialize the entire mass that will be introduced over the course of the simulation at the initial time step. Over the course of the simulation this material is pushed over the wire mass source with the wire feed speed. This treatment allows the use of the easier and generally more robust particle-particle surface tension and viscosity formulas instead of particle-boundary formulas, since there is always a layer of solid particles to interact with above the layer currently passing the mass source point.

Mass is pushed past the mass source point as specified by the direction parameter and feed speed parameters. Currently the wires are arranged in a 45° angle from the height axis (see, with two different, but constant over time, feed speeds for the first and second wire, determined from the mass fluxes $\dot{m}_{d1}$ and $\dot{m}_{d2}$, quantitatively same as realized in the FVM approach.

DROPLET DETACHMENT PROCESS

The simulation framework does not contain any models relating to electricity and its effects. This means that electromagnetic effects are not taken into account, specifically those relating to the electric arc. To facilitate droplet detachment without a physical treatment of the electromagnetic forces, droplet particles are periodically accelerated to a sufficient velocity for regular, uniform droplet detachment as observed in experiments. The detachment frequency was chosen at 100 Hz according to experimental data. Secondly, the energy gain in the wires by current running through them is also not modelled. Instead particles close to the tip of the wire have their temperature simply set to 2100 K, which conforms roughly to temperature observations of the droplet at 170 A. Through these two mechanisms orderly droplet formation and detachment are achieved.

DETERMINATION OF SURFACES

A prerequisite for the application of various boundary conditions is a determination of surfaces, mainly which particles belong to a surface, and are thus subject to these boundary conditions. While SPH is very well suited for the simulation of free moving of the particles, the actual extraction of these is a widely known problem, for which numerous differing approaches have been proposed. A very robust approach, that strikes the balance between high quality results and computational efficiency, is the so-called coverage technique [36]. First for all particles, the local coverage vector at a point $\vec{x}$ can be calculated as

$$\vec{n} = \sum_{j \in \mathcal{N}_{\vec{x}}} \left(\vec{x} - \overrightarrow{x_j} \right) \tag{42}$$

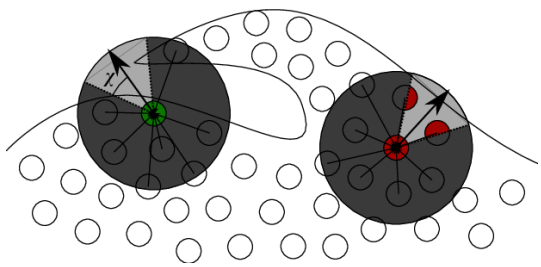

Fig. 10 Classification of surface particles using the coating method. The green particle (left) is classified as surface particle and the red particle (right) is classified as internal (not surface particle). [3]

In fully occupied regions this vector will be close to zero as all conditions are cancelled. This vector will be significantly different from 0 only in partially unoccupied regions and will be directed towards the region of the local lowest particle density. Thus, it acts as a geometric estimate of the normal vector for the local neighbourhood. The cone defined by the particle location, this local coverage vector and the angle χ can then be checked for the presence of particles. If no particles are detected within the cone, the particle is classified as a surface particle. (Fig. 10). The angle χ remains a parameter of the method, in experiments it was found that $\chi = 30^{\circ}$ leads to excellent classification results, so this value was used in all simulations.

SURFACE TENSION

To model the surface tension of the fluid, the method from [33] was used. There the surface normals are estimated using the gradient $\vec{n} = \nabla C$ of the so-called color field, defined as

$$C(x) = \sum_{j \in \mathcal{N}_{\vec{x}}} V_j \, W(\vec{x} - \overrightarrow{x_j}; h) \tag{43}$$

The color field is a simple SPH interpolation without the discretized quantity in the equation, meaning that quantity is implicitly 1 for all particles.

The resulting field is 1 in fully occupied regions, 0 in empty regions and between 0 and 1 in partially occupied regions. The gradient of this field, always pointing in the direction of maximum color gain, can be treated as a stand-in for the surface normal.

From the normals it is possible to estimate the curvature as

$$\kappa = \frac{-\nabla^2 C}{||\vec{n}||} \tag{44}$$

Given a surface tension coefficient γ, the force arising due to surface tension can then be calculated as

$$f_S = \gamma \kappa \vec{n} \tag{45}$$

Note that the used surface tension force in the actual version of simulation solver is not dependent upon temperature. This limits the model somewhat for the use in welding simulations, where temperature gradients, and associated surface tension gradients occur.

VISCOSITY & COHESION

To model the viscosity, the model presented by Weiler et al. [37], with the adaption of temperature-dependency, was used. Additionally cohesion and XSPH [38] models were integrated into viscosity model. The cohesion force acts in a similar way to the surface tension, but differs in the algorithmic formulation. Through cohesion all particles add an accelerating contribution to their neighbourhood based on the velocity difference between particles. In fully dense regions the cohesive force should equalize to 0. The XSPH method is used to alleviate noise in the particle velocities, which can be introduced by a multitude of sources, e.g. by unfavourable neighbourhoods. To avoid unwanted effects from noisy velocities, they are slightly smoothed over the neighbourhood. Note that XSPH does not add or remove momentum, it simply redistributes it over the neighbourhoods.

Both of these models were found to lead to more stable results, especially for droplets in flight, which are subject to much higher velocities than the rest of the material.

RADIATION & CONVECTION

Models for radiative and convective heat transfer are implemented. Losses through thermal radiation for a surface particle *i*, as determined by the coverage approach, are implemented in the same way as by the Eulerian approach with the equation [6], but each particle will be addressed in the SPH-method as

$$\dot{q} = \varepsilon\sigma(T^4 - T_0^4) \tag{46}$$

A heat flux between the environment and the material for a surface particle *i*, again as determined by the coverage approach is implemented as

$$\dot{q} = h(T - T_0) \tag{47}$$

To apply these heat fluxes an estimation of the exposed surface area is needed. Unfortunately, there is no model implemented within SPlisHSPlasH at the moment that can determine the exposed area of a surface particle. Such a model would require careful design, testing and an evaluation of its correctness, and would thus likely constitute a scientific contribution on its own. Therefore, both convection and radiation currently use a constant estimate of $A = (2r_p)^2$, i.e. a squared particle diameter, for the exposed surface area per particle. This estimate is accurate for flat regions, but an overestimate for concave regions and an underestimate for convex regions. Here we argue that the sue of this estimation is appropriate, since the error introduced by it, is negligible, and other parameters such as the coefficients ϵ and h, which were not subject to careful adjustment, have a far more significant impact on the final result.

LASER EFFECT

In the SPH simulation the laser is defined using a projective 2D approach. First a projection plane, from which the effect originates, is defined by an extent and a normal direction, defining the direction in which the effect is applied. For all these particle positions, multiple conditions are checked, namely are they within the dimension of the plane, i.e. can be reached from the plane by following the normal, are they in the correct direction from the plane, are their normals and the heat source normal oriented opposite, and finally are they a surface particles as determined by the coverage method [36] described above. In this manner it is possible to calculate all particles that should be effected by the heat source through local conditions, without differentiating between cladding layer and substrate particles.

Lastly the strength of the heat source influence can be defined as any two dimensional function, that exists in the plane defined at the start. After having identified all relevant particles, it is possible to project them into this plane, to calculate the point from which a ray following the normal would have originated, and evaluate the function there.

In this work the function that gives the energy distribution is an isotropic two dimensional Gaussian with the radius r_l. The energy flux for a particle i, whose projected point has a distance of r to the center of the Gaussian is therefore computed as

$$\dot{q}_i = \frac{3P}{\pi r_l^2} exp\left(\frac{-3r^2}{r_l^2}\right) \tag{48}$$

Currently, there is no variable absorption of the power based on the angle of incidence, however there is a general absorption scaling factor, currently set to 50 %.

The laser is defined in terms of a source and target point. The beam originates from the source point and is targeted toward the target point. Initially the target point is located on the substrate surface with a parametrized laser offset (see Fig. 9). The source point is located 300 mm away according to the angle φ, in accordance with the arrangement of the real process. These two points are defined relative to the wire mass source, so they move at the welding speed. Additionally, the target point oscillates sinusoidal with a frequency of 10 Hz and an amplitude of 6.6 mm along the y-axis during the simulation.

RESULTS AND DISCUSSION

The simulations in both approaches were performed on a single node on the RWTH CLAIX-18 cluster made up of two Intel Xeon Platinum 8160 “SkyLake” Processors (2.1 GHz, 24 cores each).

The LDNA simulation with FVM model used a mesh with 690K elements, 722K nodes. The smallest size of elements is 0.15 [mm] in the free surface area. Numerically, the model becomes more stable over time and the convergence of liquid and gas improves. The Root Mean Square (RMS) for convergence of fluid medium fluctuates around 1e-4 and around 1e-6 for the shielding gas.

In the FVM approach, 0.5 [s] of the process were simulated in 84h, 18m or 4046 core-hours. The wall time was not used only for calculation. This time results from 8.5% variable updates and 0.7% for writing 2500 output data and 90.8% for miscellaneous including calculation.

The SPH model consisted of 607K particles with a radius of 0.1 [mm], which were simulated for 4 [s] of LDNA process. The SPH simulation for the first second of the process took 09h, 21m on the specified hardware, simulating the entire process took 30h, 20m.

In both cases (Fig. 11), FVM (left) and SPH (right), the falling droplets into the weld pool can be seen.

The surface in the FVM is defined as Volume of fluid of 0.5. With very fine meshing, the boundaries of the VOF 0.5 and 0.9 can be close. However, in this case the need for a very fine mesh greatly increases the computation effort.

Both approaches can be used for simulating the LDNA process and show good qualitative agreement, both between SPH and FVM methods and between simulation and Experiment. For the quantitative agreement, the other parameters, including in particular surface tension and density as well as angle-dependent absorption coefficients in SPH, still have to be calibrated. The deformation of the melt surface due to the droplet momentum can be represented very well in the Euler approach. The current version's SPH approach needs to be further developed for surface effects.

For more complex droplet detachment topologies, the SPH method is better suited than the FVM. Since SPH natively ensures mass conservation and due to its mesh-free formulation, simulation of next passes in multilayer deposition welding would not lead to a significant additional computational effort.

The evaporation process is an important part of the LDNA process in reality. As such quantitative agreement between a simulation and reality would require a model in this regard. The sub-model of evaporation can be described as a combination of mass, heat loss and momentum gain. The phenomenon of heat, mass and momentum change through evaporation can be implemented very well in the Euler approach. For SPH, the decrease in heat and increase in momentum during evaporation can be taken into account, but there is currently no such model in the SPlisHSPlasH framework. The development of an evaporation model dealing with heat, mass and momentum change for SPlisHSPlasH is a further aim.

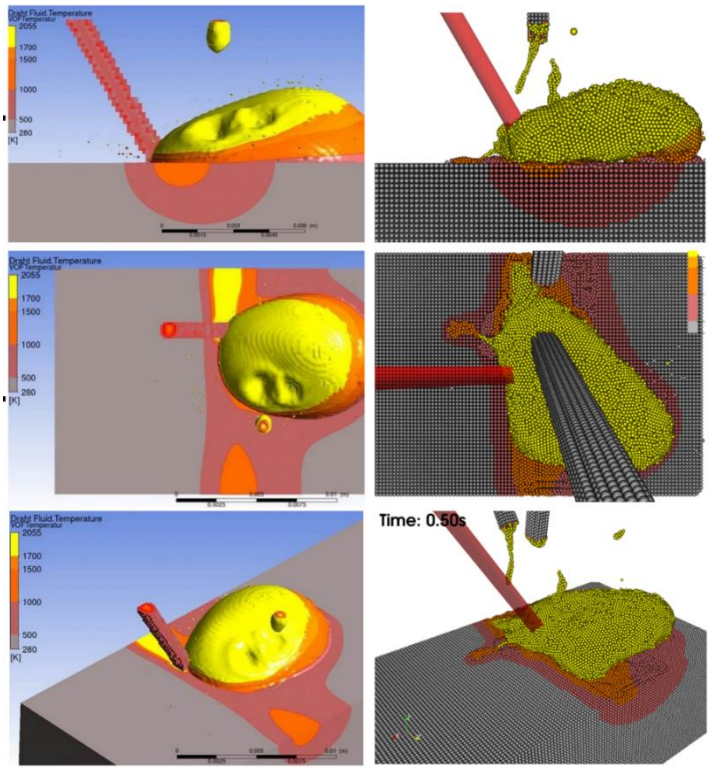

Fig. 11 The simulation results for the FVM (left) and SPH (right) methods

CONCLUSION

Both approaches offer the possibility to simulate the LDNA process. We can note a qualitative agreement, both between SPH and FVM method and between simulations and experiments. The computational resources needed for the FVM method is larger than that for the SPH method by about a factor of 17. The FVM method provides a more accurate representation of the process with physical phenomena such as evaporation, as well as surface formation and modification by the local forces present. The FVM method should be used for higher accuracies or for a fine description of surface phenomena.

The SPH method offers significantly faster simulation times for processes where flow is the dominant phenomenon, while still producing results with close agreement to FVM. It is especially suited for processes with discontinued flows. As the SPH formulation explicitly only discretizes the fluid and solid metal, the environment and its various effects are neglected.

If neglecting the effect of the protective atmosphere is acceptable for a simulation case, the simulation results for such processes could be available in a significantly shorter time and with comparable agreement.

ACKNOWLEDGMENT

The investigations have been carried out within the research project DFG 423140171. The authors would like to express their special gratitude to the German Research Foundation (DFG).

The authors gratefully acknowledge the computing time granted by the NHR4CES Resource allocation Board and provided on the supercomputer CLAIX at RWTH Aachen University as part of the NHR4CES infrastructure. The calculations for this research were conducted with computing resources under the project 20019.

References

[1] BENDER, J.: *SPlisHSPlasH*, https://github.com/InteractiveComputerGraphics/SPlisHSPlasH, 2022.

[2] S.R. JESKE, J. BENDER, K. BOBZIN, H. HEINEMANN, K. JASUTYN, M. SIMON, O. MOKROV, R. SHARMA, U. REISGEN: 'Application and benchmark of SPH for modeling the impact in thermal spraying', *Comp. Part. Mech.*, 2022, https://doi.org/10.1007/s40571-022-00459-9.

[3] S.R. JESKE, M.S. SIMON, O. SEMENOV, J. KRUSKA, O. MOKROV, R. SHARMA, U. REISGEN, J. BENDER: 'Quantitative evaluation of SPH in TIG spot welding', *Comp. Part. Mech.*, 2022, https://doi.org/10.1007/s40571-022-00465-x.

[4] A. BARROI, J. AMELIA, J. HERMSDORF, S. KAIERLE, V. WESLING: 'Influence of the Laser and its Scan Width in the LDNA Surfacing Process', *Physics Procedia*, 2014, https://doi.org/10.1016/j.phpro.2014.08.164.

[5] A. BARROI, J. HERMSDORF, U. PRANK, S. KAIERLE: 'A Novel Approach for High Deposition Rate Cladding with Minimal Dilution with an Arc – Laser Process Combination', *Physics Procedia*, 2013, https://doi.org/10.1016/j.phpro.2013.03.076.

[6] A. BARROI, F. ZIMMERMANN, J. HERMSDORF, S. KAIERLE, V. WESLING, L. OVERMEYER: 'Evaluation of the laser assisted double wire with nontransferred arc surfacing process for cladding', *Journal of Laser Applications*, 2016, https://doi.org/10.2351/1.4944001.

[7] T. BOKELMANN, M. LAMMERS, J. HERMSDORF, S. EMADMOSTOUFI, O. MOKROV, R. SHARMA, U. REISGEN, S. KAIERLE: 'Experimental setup for determination of absorption coefficient of laser radiation in molten metals as a function of temperature and angle', In: *Proceedings of Lasers in Manufacturing Conference (WLT-LiM)*, 2021, Online Conference, 21-24 June 2021.

[8] T. BOKELMANN, M. TEGTMEIER, M. LAMMERS, J. HERMSDORF, S. KAIERLE, S. EMADMOSTOUFI, O. MOKROV, R. SHARMA, U. REISGEN: 'Influence of the laser beam parameters in the laser assisted double wire welding with nontransferred arc process on the seam geometry of generatively manufactured structures', *Journal of Laser Applications*, 2021, https://doi.org/10.2351/7.0000521.

[9] M.S. AMAL, C.T. JUSTUS PANICKER, V. SENTHILKUMAR: 'Simulation of wire arc additive manufacturing to find out the optimal path planning strategy', *Materials Today*: *Proceedings*, 2022, https://doi.org/10.1016/j.matpr.2022.06.338.

[10] Y. ZHENG, Z. YU, J. XIE, J. CHEN, C. YU, J. XU, H. LU: 'A numerical model-based deposition strategy for heat input regulation during plasma arc-based additive manufacturing', *Additive Manufacturing*, 2022, https://doi.org/10.1016/j.addma.2022.102986.

[11] S.H. NIKAM, N.K. JAIN: 'Three-dimensional thermal analysis of multi-layer metallic deposition by micro-plasma transferred arc process using finite element simulation', *Journal of Materials Processing Technology*, 2017, https://doi.org/10.1016/j.jmatprotec.2017.05.043.

[12] Q. CHAI, C. FANG, J. HU, Y. XING, D. HUANG: 'Cellular automaton model for the simulation of laser cladding profile of metal alloys', *Materials & Design*, 2020, https://doi.org/10.1016/j.matdes.2020.109033.
[13] X. HAN, C. LI, X. CHEN, S. JIA: 'Numerical simulation and experimental study on the composite process of submerged arc cladding and laser cladding', *Surface and Coatings Technology*, 2022, https://doi.org/10.1016/j.surfcoat.2022.128432.
[14] L. WANG, D. ZHANG, C. CHEN, H. FU, X. SUN: 'Multi-physics field coupling and microstructure numerical simulation of laser cladding for engine crankshaft based on CA-FE method and experimental study', *Surface and Coatings Technology*, 2022, https://doi.org/10.1016/j.surfcoat.2022.128396.
[15] B. SONG, T. YU, X. JIANG, W. XI, X. LIN: 'The relationship between convection mechanism and solidification structure of the iron-based molten pool in metal laser direct deposition', *International Journal of Mechanical Sciences*, 2020, https://doi.org/10.1016/j.ijmecsci.2019.105207.
[16] A.P. SEMYONOV: 'Methods of mathematical modelling of the processes of electrode metal drop formation and transfer in consumable electrode welding', *Paton Weld J 10*, 2-10, 2014.
[17] J. HAIDAR, J.J. LOWKE: 'Predictions of metal droplet formation in arc welding', *J. Phys. D: Appl. Phys*, 1996, https://doi.org/10.1088/0022-3727/29/12/003.
[18] M. HERTEL, U. FÜSSEL, M. SCHNICK: 'Numerical simulation of the plasma-MIG process-interactions of the arcs, droplet detachment and weld pool formation', *Weld World*, 2014, https://doi.org/10.1007/s40194-013-0095-6.
[19] S. CADIOU, M. COURTOIS, M. CARIN, W. BERCKMANS, P. LE MASSON: '3D heat transfer, fluid flow and electromagnetic model for cold metal transfer wire arc additive manufacturing (Cmt-Waam)', *Additive Manufacturing*, 2020, https://doi.org/10.1016/j.addma.2020.101541.
[20] M. MEDALE, S. RABIER, C. XHAARD: 'A Thermo-Hydraulic Numerical Model for High Energy Welding Processes', *Revue Européenne des Éléments Finis*, 2004, https://doi.org/10.3166/reef.13.207-229.
[21] M. MEDALE, C. TOUVREY, R. FABBRO: 'An axi-symmetric thermo-hydraulic model to better understand spot laser welding', *European Journal of Computational Mechanics*, 2008, https://doi.org/10.3166/remn.17.795-806.
[22] M.C. NGUYEN, M. MEDALE, O. ASSERIN, S. GOUNAND, P. GILLES: 'Sensitivity to welding positions and parameters in GTA welding with a 3D multiphysics numerical model', *Numerical Heat Transfer, Part A: Applications*, 2017, https://doi.org/10.1080/10407782.2016.1264747.
[23] L.B. LUCY: 'A numerical approach to the testing of the fission hypothesis', *The Astronomical Journal*, 1977, https://doi.org/10.1086/112164.
[24] R.A. GINGOLD, J.J. MONAGHAN: 'Smoothed particle hydrodynamics: theory and application to non-spherical stars', *Monthly notices of the royal astronomical society*, 1977, https://doi.org/10.1093/mnras/181.3.375.
[25] R. DAS, P.W. CLEARY: 'Three-dimensional modelling of coupled flow dynamics, heat transfer and residual stress generation in arc welding processes using the mesh-free SPH method', *Journal of Computational Science*, 2016, https://doi.org/10.1016/j.jocs.2016.03.006.
[26] I. MASUMI, N. YU, I. SEIICHIRO, F. YU, S. MASAYA: 'Numerical Simulation of Joining Process in a TIG Welding System Using Incompressible SPH Method', *Quarterly Journal of the Japan Welding Society*, 2015, https://doi.org/10.2207/qjjws.33.34s.
[27] M. TRAUTMANN, M. HERTEL, U. FÜSSEL: 'Numerical simulation of weld pool dynamics using a SPH approach', *Weld World*, 2018, https://doi.org/10.1007/s40194-018-0615-5.
[28] H. KOMEN, M. TANAKA, H. TERASAKI: 'Three-Dimensional Simulation of Gas Metal Arc Welding Process Using Particle-Grid Hybrid Method', *Quarterly Journal of the Japan Welding Society*, 2020, https://doi.org/10.2207/qjjws.38.25s.

[29] H. KOMEN, M. SHIGETA, M. TANAKA: 'Numerical simulation of molten metal droplet transfer and weld pool convection during gas metal arc welding using incompressible smoothed particle hydrodynamics method', *International Journal of Heat and Mass Transfer*, 2018, https://doi.org/10.1016/j.ijheatmasstransfer.2018.01.059.
[30] A. D. BRENT, V. R. VOLLER, K. J. REID: 'Enthalpy-porosity technique for modeling convection-diffusion phase change: application to the melting of a pure metal', *Numerical Heat Transfer*, 1988, https://doi.org/10.1080/10407788808913615.
[31] V.R. VOLLER, A.D. BRENT, C. PRAKASH: 'Modelling the mushy region in a binary alloy', *Applied Mathematical Modelling*, 1990, https://doi.org/10.1016/0307-904x(90)90084-i.
[32] A. PATHAK, M. RAESSI: 'A three-dimensional volume-of-fluid method for reconstructing and advecting three-material interfaces forming contact lines', *Journal of Computational Physics*, 2016, https://doi.org/10.1016/j.jcp.2015.11.062.
[33] M. MÜLLER, D. CHARYPAR, M. GROSS: 'Particle-Based Fluid Simulation for Interactive Applications', 2003.
[34] M. IHMSEN, N. AKINCI, M. BECKER, M. TESCHNER: 'A Parallel SPH Implementation on Multi-Core CPUs', *Computer Graphics Forum*, 2011, https://doi.org/10.1111/j.1467-8659.2010.01832.x.
[35] J.J. MONAGHAN: 'Smoothed Particle Hydrodynamics', *Annu. Rev. Astron. Astrophys.*, 1992, https://doi.org/10.1146/annurev.aa.30.090192.002551.
[36] A. BARECASCO, H. TERISSA, C.F. NAA: 'Simple free-surface detection in two and three-dimensional SPH solver', http://arxiv.org/pdf/1309.4290v1, 2013.
[37] M. WEILER, D. KOSCHIER, M. BRAND, J. BENDER: 'A Physically Consistent Implicit Viscosity Solver for SPH Fluids', *Computer Graphics Forum*, 2018, https://doi.org/10.1111/cgf.13349.
[38] H. SCHECHTER, R. BRIDSON: 'Ghost SPH for animating water', *ACM Trans. Graph.*, 2012, https://doi.org/10.1145/2185520.2185557.